Quantitative Comparison of Drusen Segmented on SD-OCT versus Drusen Delineated on Color Fundus Photographs

Nieraj Jain,[1] *Sina Farsiu,*[1,2] *Aziz A. Khanifar,*[1] *Srilaxmi Bearelly,*[1,3] *R. Theodore Smith,*[3] *Joseph A. Izatt,*[1,2] *and Cynthia A. Toth*[1,2]

Purpose. Spectral domain–optical coherence tomography (SD-OCT) may be useful for efficient measurement of drusen in patients with age-related macular degeneration (AMD). Areas identified as drusen from semiautomated segmentation of drusen on SD-OCT were compared to those identified from review of digital color fundus photographs (CFPs).

Methods. Twelve eyes with nonneovascular AMD were prospectively imaged with digital CFP and SD-OCT. For each eye, areas on CFP in which at least two of three retina specialists agreed on drusen presence produced the composite CFP drusen map. Automated image analysis produced another CFP map. Areas identified as drusen by segmentation on SD-OCT B-scans were plotted as the SD-OCT drusen map. The CFP and SD-OCT maps were compared and agreement was quantified. Disagreement was characterized into distinct types, and the frequency of each type was quantified.

Results. There was general agreement between CFP and SD-OCT in identifying presence and absence of drusen, with mean agreement in 82% ± 9% of total image pixels. Most disagreement (80% ± 15%) occurred at drusen margins. There was a trend toward greater detection of drusen with SD-OCT in eyes with larger drusen and with hyperpigmentation. There was a trend toward greater detection of smaller drusen by CFP.

Conclusions. Good agreement was demonstrated in drusen detection between CFP and SD-OCT. Areas of disagreement underscore limitations of CFP-based measurement of drusen, particularly in the sizing of large, soft drusen. SD-OCT shows great promise as an adjunctive tool for assessing drusen burden in AMD. (ClinicalTrials.gov number, NCT00734487.) (*Invest Ophthalmol Vis Sci.* 2010;51:4875–4883) DOI:10.1167/iovs.09-4962

From the Departments of [1]Ophthalmology and [2]Biomedical Engineering, Duke University Medical Center, Durham, North Carolina; and the [3]Department of Ophthalmology, Columbia University, New York, New York.

Supported in part by Alcon Laboratories, National Institutes of Health Grants R21 EY017393 and K23 EY018895, Genentech, and The North Carolina Biotechnology Center Collaborative Funding Grant 2007-CFG-8005 with Bioptigen (all in support of The Duke Advanced Research in SDOCT Imaging [DARSI] Laboratory). SB receives research support from the National Institutes of Health.

Submitted for publication November 22, 2009; revised January 16 and March 20, 2010; accepted March 21, 2010.

Disclosure: **N. Jain**, None; **S. Farsiu**, None; **A.A. Khanifar**, iCo Therapeutics (C); **S. Bearelly**, None; **R.T. Smith**, None; **J.A. Izatt**, Bioptigen (I, E), P; **C.A. Toth**, Alcon (F), Genentech (F), Sirion Therapeutics (F)

Corresponding author: Cynthia A. Toth, Duke Eye Center, DUMC Box 3802, Durham, NC 27710; toth0004@mc.duke.edu.

Efficient phenotyping of nonneovascular age-related macular degeneration (AMD) is an increasing priority as clinical management of the disease evolves. Drusen are a defining feature of AMD, and numerous longitudinal studies have demonstrated positive correlations between estimated total drusen area and maximum drusen size with risk of progression to advanced AMD.[1–5] These parameters are now commonly used in establishing entry criteria and endpoints for disease progression in clinical trials.[1–4]

Presently, evaluation of color fundus photographs (CFPs) represents the gold standard for drusen measurement in nonneovascular AMD. Total drusen area and maximum drusen size are estimated by visual inspection of drusen in CFPs, with comparison to a set of standardized circles.[6–8] However, it can be challenging to reliably localize drusen against the varying background of the pigments of the macula, retinal pigment epithelium (RPE), and choroid.[6,9,10] Furthermore, although reduction of drusen properties into categorical data increases the efficiency of manual CFP grading and statistical analysis, it may be an oversimplification in the evaluation of drusen burden.

Optical coherence tomography (OCT) provides in vivo imaging of drusen in cross section. Recent spectral domain OCT systems (SD-OCT), with their increase in imaging speed over conventional OCT, obtain more than 100 high-resolution scans in the time required to capture less than 10 time-domain scans.[11–14] Thus, SD-OCT represents a promising alternative modality for imaging drusen. Khanifar et al.[15] demonstrated that SD-OCT provides novel information regarding drusen ultrastructure in vivo. Schuman et al.[16] detected and quantified decreased photoreceptor layer (PRL) thickness over drusen as seen in SD-OCT images of AMD patients. Furthermore, using a summed-voxel projection[17] (SVP) of a series of B-scans of the posterior pole, an en face representation of SD-OCT reflectivity can be registered to CFPs to provide an area map of drusen segmented on OCT (see Fig. 1).[18] In a proof of concept, Yi et al.[19] used SD-OCT to quantify drusen area and volume in a patient with nonneovascular AMD.

Currently, there is no comparative study as to how sites identified as drusen with SD-OCT relate to the size and area of lesions identified as drusen on CFP. It is important to understand this relationship if drusen measurement from SD-OCT analysis is to be used in future studies. The purpose of this study was to compare areas designated as drusen from SD-OCT images with those designated as drusen on CFPs in the maculas of patients with high-risk nonneovascular AMD. We performed a quantitative comparison of total drusen area and maximum drusen size identified with the two modalities. We hypothesized that drusen extent determined with SD-OCT would correlate with findings on CFP. Differences between the two were explored.

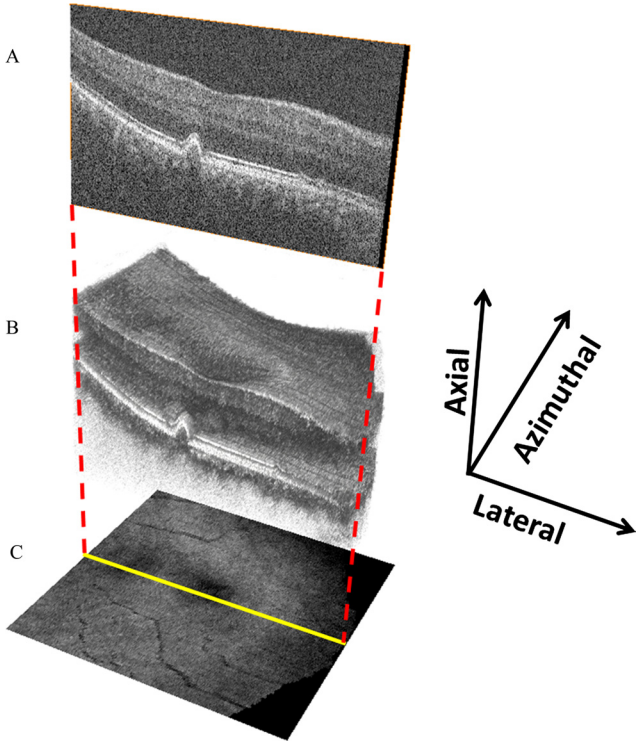

FIGURE 1. SD-OCT volume scan with SVP representation. B-scans (**A**), taken sequentially at a fixed azimuthal interval (66 μm) across the macula, form a volume scan (**B**). The three-dimensional appearance of drusen becomes apparent with volume scanning. The volume scan can be collapsed axially, with averaging of pixel intensity, to form the en face SVP retinal image (**C**).

MATERIALS AND METHODS

Data Collection

All subjects provided informed consent to participate in the Age-Related Eye Disease Study (AREDS) 2 and the AREDS2 Ancillary SD-OCT Study. For inclusion in the study, subjects had a clinical diagnosis of AREDS Category 3 nonneovascular AMD. This study was approved by the Duke University Health System Institutional Review Board, and the study protocol adhered to the tenets set forth in the Declaration of Helsinki. The enrollment period for this pilot study extended from March 27, 2007, to February 21, 2008.

Twelve eyes of 12 patients with AREDS Category 3 AMD were prospectively imaged with nonstereoscopic digital CFP (model 450; Carl Zeiss Meditec Inc., Dublin, CA) and with SD-OCT (Bioptigen Inc., Research Triangle Park, NC). Each SD-OCT image set was acquired over a 6.6 × 6.6-mm area with 100 B-scans obtained in approximately 5 seconds. Each B-scan consisted of 1000 A-scans, with a 66-μm interval between consecutive B-scans. For each set of 100 B-scans, the volume was averaged axially to produce a 100 × 1000-pixel SVP retinal image (Fig. 1).[17] Calibration of pixel size was based on 6.6 × 6.6-mm scanning protocol used by an FDA-approved SD-OCT unit (Bioptigen, Research Triangle Park, NC). The eyes in this study were not profoundly hyperopic or myopic.

Drusen Grading Protocols

Three retina specialists at Duke University independently marked all areas that they thought were drusen on each digital CFP (*Pencil* tool, Photoshop; Adobe Systems, Inc., San Jose, CA). Analysis was confined to a macular area of approximately 2-mm in diameter, centered on the fovea. A composite CFP drusen map was then created by identifying all areas in which at least two of three graders agreed on the presence of drusen (Fig. 2). Unless otherwise stated, the composite CFP map was used to represent the CFP drusen markings for comparative analysis in this study.

In addition to manual segmentation, we used software to detect and segment drusen on CFP images in an automated fashion.[20] This software was developed and implemented by the Columbia University team without knowledge of the drusen identification rules or results from the manual grading at Duke University. The automated approach used a detailed mathematical model based on the geometry of fundus reflectance reconstructed individually for each image to correct macular background and illumination variability.[21] Highly reflective structures, such as nerve fiber layer bundles at the arcades, retinal pigment epithelium (RPE) hypopigmentation, and exudates, are more frequently mistaken for drusen by an automated method than by an expert grader, requiring postprocessing steps. Consequently, we developed a more efficient user-interactive method, in which the user initially selects areas of interest from drusen images, excluding unwanted reflective structures a priori. The algorithm then computes the background model and final drusen segmentation of the macula, recognizing the absence of drusen beyond the region of interest (ROI; Fig. 3). This method permits the capture of even low-contrast lesions by uniform thresholds and has been validated and used to quantify the relationship between drusen, autofluorescence (AF), and AMD disease progression.[21–23] All algorithms were implemented in a graphical user interface (GUI) written and compiled in commercial software (MatLab; The MathWorks Inc., Natick, MA) as a free-standing executable.

Automated drusen segmentation for the SD-OCT images was performed using the Duke OCT Retinal Analysis Program (DOCTRAP).[24] The DOCTRAP algorithm detects and segments retinal layers such as the retinal nerve fiber layer (RNFL) inner boundary and the RPE using

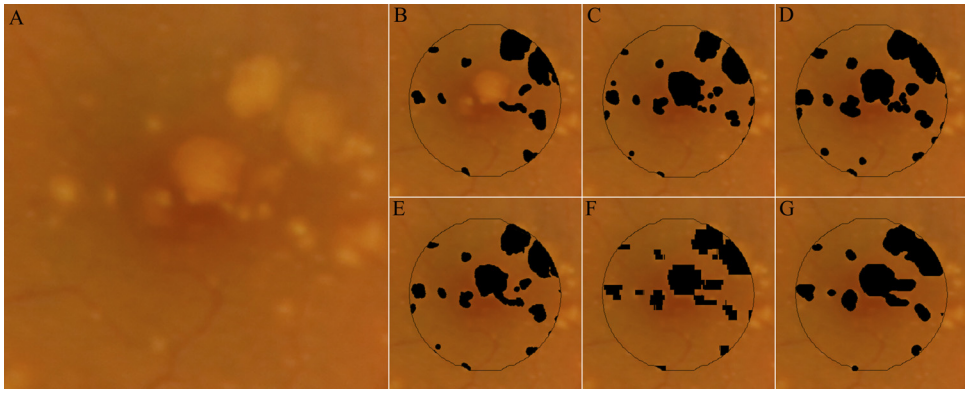

FIGURE 2. Drusen maps for study eye 3. Three retinal specialists independently graded the CFP (unmarked in **A**) for drusen (**B–D**). A composite CFP drusen map, representing all areas marked as drusen by at least two of three graders, is represented as (**E**). To create a projection map of drusen from SD-OCT scans, interpolation of sequential OCT B-scans must be performed. This is because the 6.6 × 6.6-mm field-of-view is sampled by 100 OCT B-scans. Whereas the field of view is represented by 1000 × 1000 pixels in the CFP images (**A**), there are only 100 × 1000 pixels in the projected OCT markings. (**F**, **G**) The interpolated OCT markings using a 2-D cubic interpolation function (MatLab; The MathWorks) and NWE interpolation. Unless otherwise stated, the NWE interpolation (**G**) was used for comparative analysis in this study.

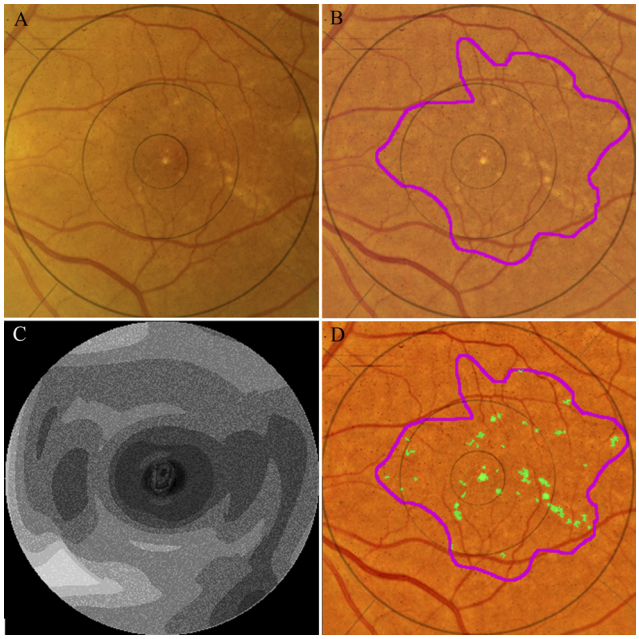

FIGURE 3. Automated segmentation of drusen on CFP. The original image (**A**) demonstrates poorly defined drusen and pigmentation variations. The image is first enhanced and color balanced, and the drusen region of interest is interactively selected (**B**). The mathematical model for the image background (contour graph, **C**) is calculated in commercial software (MatLab; The Mathworks). On the background-leveled image (**D**), the drusen detection algorithm identifies multiple drusen (*green*).

a modified implementation of the deformable contours method.[25] DOCTRAP software identifies suspect drusen areas based on irregularities in the RPE contour. An expert SD-OCT reader refined drusen segmentation on each B-scan in the study.

Several manual adjustments were made to the DOCTRAP drusen segmentation, including (1) adjustment of the lateral extent of marked drusen to correspond to the point at which the RPE deflection returned to baseline; (2) manual delineation of drusen not identified by the DOCTRAP software because of a minimal or atypical distortion of the RPE layer; and (3) removal of zones of improper segmentation in which drusen were falsely identified by DOCTRAP software. Manual refinement was performed in approximately 10 minutes for each set of 100 B-scans. This step on average accounted for an alteration in grading of 4% ± 3% of total pixels in the central macular area on the SD-OCT drusen map.

To grade drusen size, a measuring tool (Photoshop Measure tool; Adobe Systems, Inc.) was used to manually measure the diameter of the largest druse present (Fig. 4). This task was performed on both the composite CFP and SD-OCT drusen maps. In the case of confluent drusen, the maximum linear span of contiguous drusen was measured.

Image Interpolation and Registration

Because of the limited SD-OCT B-scan sampling in the azimuthal direction (Fig. 1), interpolation of the SD-OCT drusen markings was performed to estimate drusen extent between consecutive B-scans. That is, to match the size of the CFP images, SVP retinal images were interpolated to contain 1000 × 1000 pixels.

We implemented two interpolation techniques (Fig. 2). We initially used the 2-D data interpolation function (*interp2* function with *cubic* parameter; MatLab, The MathWorks). Because of the asymmetric resolution enhancement factors (factor of 10 in the azimuthal and of 1 in the lateral direction), this function in effect simplified to a 1-D interpolation in the azimuthal direction, resulting in stepwise sharp discontinuities in the interpolated SD-OCT drusen map. As an alternative approach to acquire a smoother reconstruction, we used the 2-D Nadaraya-Watson estimator (NWE) with a Gaussian kernel of size 21 × 21 and variance of 6 pixels.[26] These interpolated images were thresholded to create binary drusen maps. For each image, we adaptively selected the threshold so that the ratio of drusen versus nondrusen area would be equal in the interpolated and noninterpolated SVP images (of size 1000 × 1000 and 100 × 1000 pixels, respectively). Unless otherwise stated, this SD-OCT drusen map with the NWE interpolation is used to represent the SD-OCT drusen markings for comparative analysis in this study.

Retinal images were imported into the image analysis software (Photoshop; Adobe Systems, Inc.) and coregistered manually by adjustment of the CFP with respect to the SVP (*free transform* tool; Adobe Systems, Inc.). Using this function, we translated, rotated, scaled, and skewed the CFP image to closely register these images. As our main goal was to register the central macular area, which occupies approximately 7% of the total image area, particular attention was paid to ensuring the proper alignment of all vascular features that immediately surround this area. We noted that, even if such rigid warping transforms do not perfectly represent the global warping between these two images, they efficiently approximate the local warping transform in this small central region. Several co-authors (NJ, SF, AAK, CAT) inspected each image set to confirm that the co-registration was robust.

Analysis Protocol

Intergrader agreement for the three separate manual gradings of the CFPs was assessed at the level of individual pixels. Pairs of the CFP grading masks were overlaid in the image analysis software (Photoshop; Adobe Systems, Inc.) and subtracted to localize areas of agreement and disagreement in drusen identification. Pixel counts for agreement and disagreement were quantified (MatLab; The MathWorks). In similar fashion, agreement and disagreement were computed for the two primary measurement techniques: the composite (agreement by any two of three graders) CFP drusen map versus the SD-OCT drusen map.

Areas of disagreement in drusen identification between the composite CFP map and the SD-OCT drusen map were evaluated to identify the most frequent types of disagreement. Four broad categories of

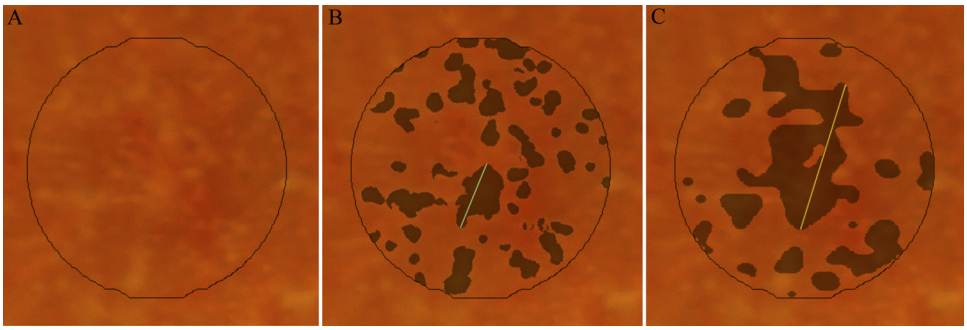

FIGURE 4. Maximum drusen size within the central study area for subject 6. Maximum drusen size is defined as the greatest linear span of contiguous drusen. (**A**) Unmarked CFP; (**B**, **C**) composite CFP and SD-OCT drusen maps, respectively, with a line indicating maximum drusen size for each drusen map.

Table 1. Total Area of Drusen within a 3.11-mm^2 Macular Study Area for Each Imaging Modality for All 12 Subjects

	SD-OCT			CFP				
	2D Interpolation		NWE Interpolation	Automated	Composite (Any 2 of 3 Graders)	Grader 1	Grader 2	Grader 3
Eye	(mm^2)	%	(mm^2)	(mm^2)	(mm^2)	(mm^2)	(mm^2)	(mm^2)
1	0.3	9	0.2	0.5	0.5	0.6	0.5	0.5
2	0.6	19	0.6	0.8	0.8	0.9	0.9	1.0
3	0.6	19	0.6	0.6	0.6	0.4	0.6	0.7
4	0.7	22	0.7	0.6	0.6	0.8	0.6	0.7
5	0.7	23	0.7	0.9	1.0	1.0	1.0	1.0
6	0.9	29	0.9	0.7	0.8	1.0	0.7	1.1
7	1.0	32	1.0	0.7	0.9	1.4	0.9	0.7
8	1.2	39	1.2	0.9	1.1	0.9	1.2	1.3
9	1.8	58	1.9	1.6	1.4	1.6	1.2	1.4
10	2.3	75	2.4	1.9	2.0	2.0	2.0	1.9
11	2.3	73	2.4	2.3	1.8	1.9	1.7	1.9
12	3.0	95	3.0	2.7	3.1	3.1	2.2	3.1
Mean	1.3	41	1.3	1.2	1.2	1.3	1.1	1.3
SD	0.9	28	0.9	0.8	0.8	0.8	0.6	0.7

For the SD-OCT drusen map, drusen markings on a series of 100 B-scans across the macula were projected onto an SVP retinal image with interpolation of spaces between sequential scans to produce a map of drusen marking by SD- OCT (see Figs. 1, 2). The automated CFP map utilized a drusen detection algorithm to identify drusen on an enhanced, background-leveled CFP image (see Fig. 3). In addition, three retinal specialists independently graded CFPs for drusen. The composite CFP map includes all areas marked as drusen by at least two of three graders (see Fig. 2). The area of drusen expressed as a percentage of the study area is reported for one set of results (column 1, SD-OCT 2-D interpolation).

disagreement were assessed, based on simultaneous inspection of the CFP and corresponding SD-OCT B-scans: (1) disagreement at margins just outside of areas in which both modalities agree "yes" for drusen; (2) hypopigmentation on CFP without a corresponding finding on SD-OCT; (3) pigment migration with obscuration of underlying drusen on CFP; and (4) drusen-shaped lesions on OCT without a corresponding finding on CFP. Each pixel of disagreement was assigned to a specific category, and manually marked with a labeling color. This analysis was performed by one grader (NJ), and all areas of marking were reviewed with agreement by a second grader (CAT). The color-coded image of disagreement was then imported into the quantitation program (MatLab; The MathWorks), and the relative frequency of each type of disagreement was quantified.

Statistical Methods

The mean and SD of the total area identified as drusen is reported for each grading modality. Similar data are presented for each type of disagreement, as a percentage of total disagreement. An intraclass correlation coefficient (ICC) was computed (SAS statistical software; SAS Institute, Cary, NC) for pairs of grading modalities. A paired Student's *t*-test was used to compare drusen size measurements between modalities. A Bland-Altman plot for drusen area was constructed for the two primary drusen maps: the composite CFP map and the SD-OCT (with NWE interpolation) map.[27]

Results

Extent of the Drusen Area

We quantified and compared drusen area with CFP- and SD-OCT-based measurement in 12 subjects. The area of drusen ranged from 0.2 to 3.0 mm^2 by SD-OCT (7%–97% of the central macular area); 0.5 to 3.1 mm^2 by composite CFP (16%–99.5%); and 0.5 to 2.7 mm^2 by automated segmentation of drusen on CFP (16%–88%). Mean drusen area was 1.3 ± 0.9 mm^2 by SD-OCT, 1.2 ± 0.8 mm^2 by composite CFP, and 1.2 ± 0.8 mm^2 by automated segmentation of CFP (Table 1). There was a trend for SD-OCT-based grading to identify a greater area of drusen as the total drusen area increased (Fig. 5). The ICC for drusen area between SD-OCT and composite CFP was 0.94 (95% CI, 0.81–0.98; Fig. 6). In contrast, the mean ICC for comparison among the three independent CFP graders was 0.90 ± 0.05.

Across this wide range of drusen size and area, grading by SD-OCT and composite CFP on average agreed on the classification of 82% ± 9% of pixels. Another 10% ± 8% of pixels were determined to be drusen with SD-OCT and not composite CFP, and 8.0% ± 4% were determined to be drusen with composite CFP and not SD-OCT (Fig. 7). Of the total area across all eyes identified as drusen with composite CFP, 80% of pixels were also identified as drusen with SD-OCT. In comparison, of the total area identified as drusen with SD-OCT, 75% of pixels were

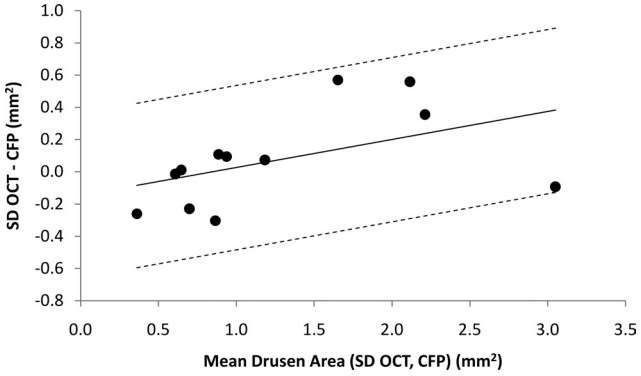

Figure 5. Bland-Altman plot for agreement between SD-OCT-based and composite CFP-based measurement of total drusen area within the central macular area in 12 subjects with AREDS category 3 nonneovascular AMD. To obtain this plot, the difference in total drusen area as measured with SD-OCT (NWE interpolation) and composite CFP was plotted against the mean drusen area of the two measurements for each subject. A modified Bland-Altman plot, using a regression approach for nonuniform differences, accounts for the positive correlation between difference in measured drusen area and mean drusen area.[27] The regression line is displayed along with the upper and lower 95% limits of agreement.

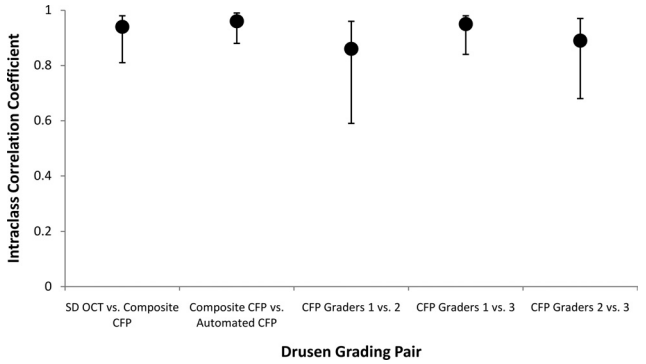

FIGURE 6. ICC for total drusen area measurement for pairs of grading modalities, along with confidence intervals.

also identified as drusen with composite CFP. The relative agreement between markings on SD-OCT versus CFP was similar to the intergrader agreement in delineating drusen on CFP, which had a mean agreement of 82% ± 6% of total image area.

The greatest linear span of a contiguous druse was consistently greater with SD-OCT than with composite CFP. The mean size of the largest druse by SD-OCT was 1286 ± 555 μm; the mean size of the largest druse by composite CFP was 915 ± 501 μm (Table 2). The mean difference was 371 μm (P = 0.008).

Interpolation Results

Segmentation of drusen on OCT demonstrated a mean drusen area of 1.3 ± 0.9 mm^2 for both the NWE interpolation and the 2-D interpolation. Varying the interpolation strategy of the SD-OCT drusen markings led to a change in 5% ± 2% of total pixels. Both strategies resulted in a similar level of agreement when compared with the drusen markings on the composite CFP map (82% agreement for NWE vs. 81% agreement for the 2-D interpolation).

Disagreement Types

Areas of disagreement in marking of drusen with SD-OCT versus composite CFP were grouped into four distinct types

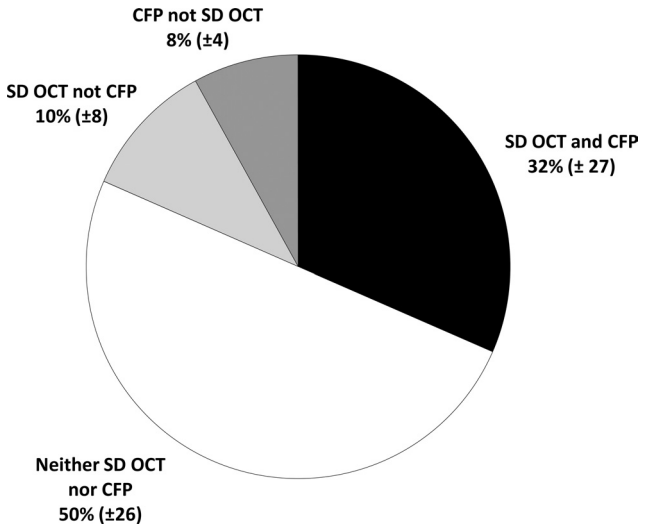

FIGURE 7. Mean agreement and disagreement for grading of drusen by SD-OCT (NWE interpolation) and composite (agreement by any two of three graders) CFP. Data reported include mean percentage of pixels (±SD) marked as drusen by both SD-OCT and composite CFP, neither SD-OCT nor CFP, SD-OCT but not CFP, and CFP but not SD-OCT.

TABLE 2. Maximum Drusen Diameter for Each of 12 Eyes, as Determined on the SD-OCT (NWE interpolation) and Composite CFP Drusen Maps

Eye	SD-OCT Max Length (μm)	CFP Max Length (μm)	Difference (SD-OCT − CFP) (μm)
1	330	340	−10
2	690	600	90
3	900	690	210
4	1000	690	310
5	1010	700	310
6	1160	520	640
7	1220	830	390
8	1300	1240	60
9	1880	670	1210
10	1980	1760	220
11	1980	960	1020
12	1980	1980	0
Mean	1286	915	371 (P = 0.008)
SD	555	501	395

For confluent drusen, the maximum length of contiguous drusen is reported (see Fig. 4). The P-value reported is obtained by paired Student's t-test.

(Figs. 8, 9). Most of the disagreements occurred at the margins just outside of areas in which both modalities agreed "yes" for drusen (Table 3). This broad category of disagreement (type I) occurred in each of the 12 eyes and accounted for 80% ± 15% of all pixels with disagreement. In these areas with type I disagreement, the CFP and corresponding SD-OCT scans were inspected to provide an estimate of the true extent of the drusen. On the basis of this estimate, it was determined that, in each instance, the CFP grading had undermarked drusen (disagreement subtype IA, royal blue), the SD-OCT grading had undermarked drusen (disagreement subtype IB, light blue), or the modality that represented the true extent of drusen was indeterminate (disagreement subtype IC, orange). A scatterplot of area of disagreement attributed to subtypes IA and IB against total drusen area shows inverse trends for these two important types of disagreement in marking drusen borders (Fig. 10).

Another type of disagreement (type II, light green) consisted of small areas of hypopigmentation identified as drusen

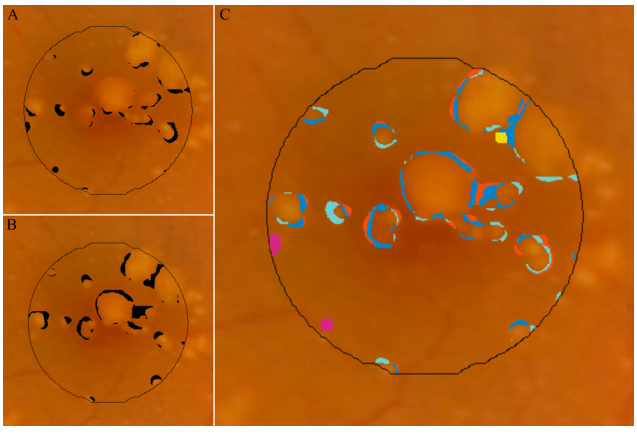

FIGURE 8. Disagreement in marking of drusen between the SD-OCT (NWE interpolation) versus composite CFP (agreement by any two of three graders) drusen maps. (**A**) Pixels identified as drusen by composite CFP but not SD-OCT; (**B**) pixels identified as drusen by SD-OCT but not CFP; (**C**) color coding of pixels by various subtypes of disagreement (see Table 3).

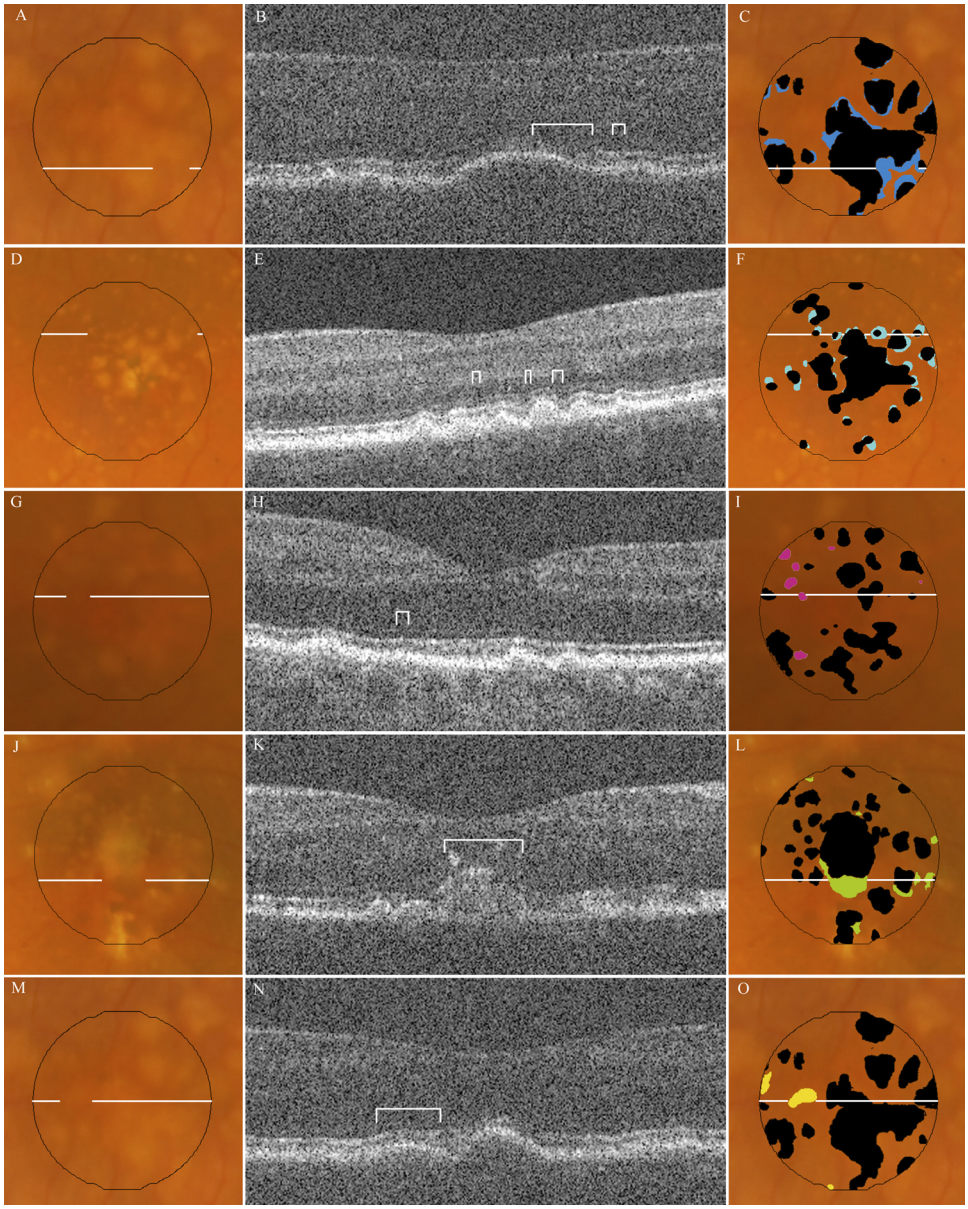

FIGURE 9. Types of disagreement in drusen identification by SD-OCT and CFP. *Left column*: CFPs for representative examples of disagreement, each with an outline indicating location of the corresponding B-scan. *Middle column*: the SD-OCT B-scan for each sample, with *brackets* identifying the region of disagreement. *Right column*: the same fundus photo with either the SD-OCT map (**F**, **I**) or composite CFP drusen map (**C**, **L**, **O**) in *black*, superimposed with color markings representing all areas of the specified disagreement type (see Table 3): (**A–C**) type IA, undermarking of drusen borders by CFP; (**D–F**) type IB, undermarking of drusen borders by SD-OCT; (**G–I**) type II, hypopigmentation with appearance of drusen without a corresponding OCT finding; (**J–L**) type III, pigmentary migration with obscuration of underlying drusen; and (**M–O**) type IV, OCT deflection without corresponding CFP pigmentary change. (Not pictured: type IC, nonspecific disagreement at drusen borders.)

on CFP, but with no corresponding finding on SD-OCT. These "drusen" had a maximum diameter of 220 μm, with a median diameter of approximately 70 μm. This type of disagreement occurred in 11 of 12 eyes, and accounted for 10% ± 10% of total disagreement by area.

There were two different findings at the sites of type II disagreement. In the majority of such instances (73/99), the lesions were greater than 60 μm in diameter and appeared to have an SD-OCT scan across the location, with minimal to no disturbance of the RPE contour on the B-scan. In the remaining 26 of 99 such instances, we suspect that drusen were undetected on SD-OCT because of the unsampled space (~40 μm, presuming a 15-μm-wide diameter site sampled by the SD-OCT beam at the retina) between adjacent B-scans. In these cases, inspection of other SD-OCT scans of the same eye at greater resolution can visibly demonstrate a subtle deflection of RPE in the area corresponding to the lesion on the CFP.

A third type of disagreement (type III, dark green), occurred at regions where pigment migration or hyperpigmentation masked the presence of drusen on the CFP. SD-OCT scans documented the extent of drusen material (often large confluent drusen) beneath hyperreflective zones corresponding to the site where drusen were not marked on CFP. This type of disagreement accounted for a mean of 6% ± 9% of total disagreement, and occurred only in the five eyes with such pigmentary changes. However, in these eyes, this type of disagreement accounted for a mean of 13% ± 9% of total disagreement, and as much as 24% of the total disagreement. In one subject, not only did hyperpigmentation obscure 16% of the total drusen area, but outside the central macular area, a large area of hypopigmentation masqueraded as a large druse (Fig. 11). In these instances, drusen measurement with SD-OCT appeared to be more accurate than with CFP.

A fourth type of disagreement (type IV, yellow) consisted of areas clearly demonstrating drusen on the SD-OCT B-scan without a visible appearance of drusen on CFP. To contrast with type III disagreement, in these instances there was no associated hyperpigmentation to account for the masking of drusen on CFP. This disagreement type occurred in 9 of 12 eyes, accounting for 5% ± 5% of total disagreement.

TABLE 3. Disagreement Types with Corresponding Color Code

Color	Type	Description of Disagreement Type	Eyes (*n*)	Mean % of Disagreement
	IA	Undermarking of drusen borders by CFP	12	35 ± 21
	IB	Undermarking of drusen borders by SD-OCT	12	27 ± 14
	IC	Nonspecific disagreement at drusen borders	12	18 ± 13
	II	Hypopigmentation on CFP without SD-OCT finding	11	10 ± 10
	III	Pigmentary migration with obscuration of underlying druse	5	6 ± 9
	IV	SD-OCT deflection without corresponding pigmentary change	9	5 ± 5

Disagreement between SD-OCT and composite CFP drusen maps were evaluated at each image pixel for all 12 subjects (see Fig. 9). Four major types of disagreement are reported. A brief description of each type of disagreement is presented in the middle column. For each type, area is reported as the mean percentage of the total disagreement ± SD.

DISCUSSION

SD-OCT is a novel imaging modality for quantifying drusen size and area in patients with AMD. The high-resolution and limited motion artifact in SD-OCT scans makes possible a precise characterization of drusen extent with sequential scanning across the macula. In this study, we validate the accuracy of this technique by comparison to the prevailing standard of CFP-based drusen measurement.

We report the first quantitative comparison of drusen area measurement by SD-OCT versus CFP. Our findings corroborate our hypothesis that drusen area as determined with SD-OCT will be similar to area determined with CFP. Of interest, drusen grading with SD-OCT appeared to have increased sensitivity in subjects with greater total drusen burden, as is depicted in the Bland-Altman plot (Fig. 5).

Comparison of disagreement between SD-OCT-based versus CFP-based marking of drusen at the level of individual pixels is highly informative. Most lesions that are classically interpreted as drusen on CFP had corresponding findings on SD-OCT, and vice versa. The predominant type (type I) of disagreement occurred at the boundaries of regions identified as drusen by both modalities. This disagreement type accounted for 80% ± 15% of total disagreement between the two modalities and also accounted for the notable disagreement in largest drusen size between the two modalities.

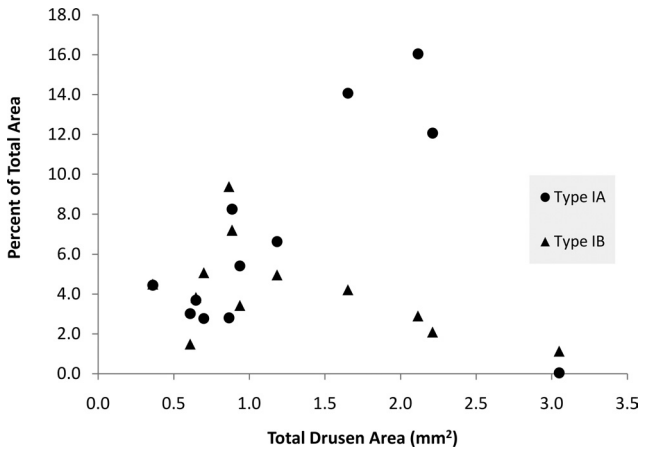

FIGURE 10. Disagreement types IA and IB, represented as a percentage of the total area of interest, are plotted against total drusen area (average of SD-OCT- and CFP-based measurements) for each of 12 subjects (see also Fig. 9, Table 3).

The difficulty in precisely identifying the borders of drusen represents an important challenge. A high degree of precision is needed if we are to use either CFP or SD-OCT as a tool to monitor disease longitudinally. We argue that SD-OCT offers greater precision for patients with advanced disease. Cross-sectional images of drusen at the axial resolution offered by SD-OCT and with the sampling density selected for this study provide much greater detail regarding borders of large, soft drusen than can be extracted from inspection of CFPs. In contrast, for tiny and sharply delineated, small, hard drusen, CFP offers an advantage in imaging over SD-OCT scanning at 66-μm intervals. Precise characterization of higher risk large drusen is likely to be more valuable in the clinical setting.

This strength of SD-OCT is also supported by quantitative data from our study. In subjects with the greatest drusen burden, in whom drusen merged to form large confluent lesions, there was an increasing proportion of type IA disagreement (undermarking of drusen borders by CFP; Fig. 10). Type IA disagreement represents the subtype with greatest contribution to overall disagreement between the two modalities (35% ± 21% of total disagreement). This disagreement subtype is also largely responsible for the difference in maximum drusen size, where measurements on SD-OCT are consistently greater than those on CFP (Table 2).

Disagreement type II, representing sites of hypopigmentation on CFP without a corresponding finding on OCT, encompasses a group of relatively small lesions. In the most cases, whether these lesions represent true drusen versus nonspecific hypopigmentation is indeterminate. This lack of a clear identification again underscores limitations in CFP-based grading of drusen, which relies heavily on macular pigmentary changes as a sign of drusen presence, despite the increased frequency of pigmentary changes such as RPE atrophy, hyperplasia, and migration in AMD.

In less than half of such cases, we suspected that sites with type II disagreement represented true drusen that were undetected with SD-OCT because of the spacing between adjacent B-scans in our imaging protocol. Greater sampling density has been shown to increase detection of small drusen (Farsiu S, unpublished data, 2008). For this study population with AREDS category 3 AMD, as shown by our quantitative analysis, this sampling frequency did not introduce substantial disagreement between SD-OCT- and CFP-based grading of drusen. The issue of undersampling may be more significant if SD-OCT were used

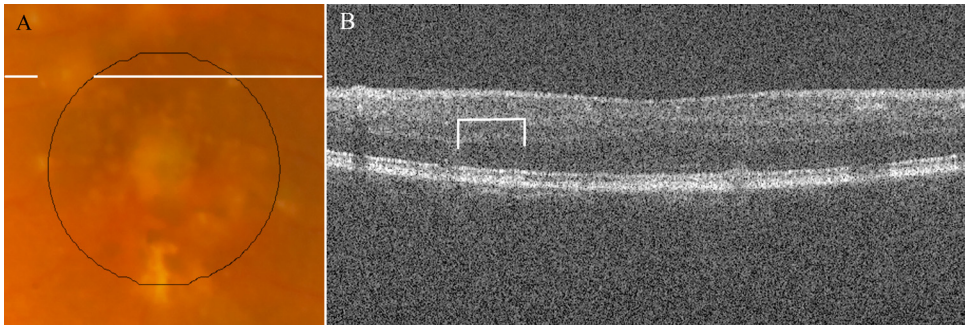

FIGURE 11. The lines on the CFP (**A**) highlight an area marked as drusen by all three CFP graders, just outside the central macular area of interest. The corresponding SD-OCT B-scan (**B**) did not reveal drusen at this location, highlighted with brackets.

in the assessment of drusen burden in early AMD. Further study of SD-OCT with greater B-scan sampling would clarify the utility of this imaging modality in patients with early AMD.

Type III and IV disagreements also resulted from the overreliance of CFP-based grading on pigmentary changes for drusen identification. Type III disagreement accounted for instances in which drusen were concealed by overlying pigmentary changes. In type IV disagreement, lesions with clear drusenoid RPE deflection on OCT did not produce a corresponding pigmentary change that was recognized as drusen on CFP.

The ultimate goal for SD-OCT-based drusen measurement would be to have fully automated segmentation of drusen on SD-OCT. In this study, we performed semiautomated segmentation to evaluate the optimal performance of SD-OCT in quantifying drusen. The intent was to avoid major segmentation errors that would significantly sway the results. Refinement of automated segmentation on SD-OCT B-scans was performed rapidly and had surprisingly little effect on ultimate drusen area measurements. A total of 4% ± 3% of pixels was altered by manual refinement of SD-OCT drusen markings.

In completing the SD-OCT-based measurement of drusen area, we used the NWE interpolation strategy to up-sample our 100 linear B-scans to span the 1000 pixels vertically across the macula. This interpolation strategy was chosen to model the natural tendency of drusen to have curvilinear borders. We also performed the analysis using a more simplistic 2-D interpolation (MatLab; The MathWorks) to examine the influence of interpolation strategy on the results. Our analysis demonstrated that, although it visually appeared to have greater agreement, the NWE interpolation strategy had only a minor influence of on ultimate agreement with CFP drusen markings.

A potential challenge in this type of study is that there is no gold standard for measurement of drusen area. Aware of this limitation, we used statistical methods that do not rely on comparison to a gold standard. Furthermore, we chose to use a composite CFP drusen map, defining drusen and nondrusen areas as sites where any two of three graders agreed, to minimize the potential bias introduced by any one grader. We checked this composite grading against a previously published method of automated segmentation of drusen on CFP[21] and found remarkably similar results.

One limitation of this pilot study is the small sample size. However, the 12 subjects in the study represented a broad sampling of AREDS category 3 AMD phenotypes. A variety of different drusen morphologies and sizes were present. Drusen area ranged from 7% to 97% of our central macular area by SD-OCT. A further limitation is that accurate comparison between two different imaging modalities at the level of individual pixels necessitates accurate co-registration of the CFP and SVP retinal image. Fortunately, the SVP retinal image offers many landmarks in the form of vessel shadows to properly co-register the images. To maximize agreement between images, rather than using automated image registration techniques, we co-registered all images manually. Inaccuracies in image co-registration, however small, would reduce the overall level of agreement in drusen identification between the two modalities.

This study provides a comparison of SD-OCT- and CFP-based drusen measurement at a single time point and does not provide longitudinal data. In addition, we did not perform drusen volume measurements in this study, as this information cannot be quantified in CFP analysis. The capacity for SD-OCT to provide volume measurements is a unique feature of this imaging modality that we are actively studying.

Combined analysis of both the qualitative characteristics of drusen[15] and quantitative measurements from SD-OCT imaging of the macula in AMD is very likely to result in improved characterization of the AMD phenotype. For example, the AREDS severity scale combines both qualitative and quantitative drusen characteristics in a stepwise scale that correlates with greater risk of progression to advanced disease.[2] Klein et al.[28] have shown patterns of drusen or pigment on CFP that are likely to precede geographic atrophy. The utility of SD-OCT analysis to precisely identify disease stage and predict risk of future progression to advanced disease and vision impairment remains to be demonstrated in a longitudinal study. These questions will be examined in the longitudinal 5-year Age-Related Eye Disease Study 2 Ancillary SD-OCT Study.[29]

Drusen area and size measurements are unmistakably correlated with disease progression in nonneovascular AMD. Advances in the management of AMD demand a level of precision in both clinical trials and the clinical setting that is not possible with color photography alone. The results in this pilot study show that SD-OCT can be an important tool in measuring the extent of drusen and offers the potential for greater precision and efficiency than does CFP alone.

Acknowledgments

The authors thank Sandra Stinnett for assistance with statistical analysis and the Age Related Eye Disease Study 2 for its support.

References

1. Klein R, Klein BE, Tomany SC, Meuer SM, Huang GH. Ten-year incidence and progression of age-related maculopathy: The Beaver Dam eye study. *Ophthalmology.* 2002;109:1767–1779.
2. Davis MD, Gangnon RE, Lee LY, et al. The Age-Related Eye Disease Study severity scale for age-related macular degeneration: AREDS Report No. 17. *Arch Ophthalmol.* 2005;123:1484–1498.
3. Wang JJ, Foran S, Smith W, Mitchell P. Risk of age-related macular degeneration in eyes with macular drusen or hyperpigmentation: the Blue Mountains Eye Study cohort. *Arch Ophthalmol.* 2003;121:658–663.
4. van Leeuwen R, Klaver CC, Vingerling JR, Hofman A, de Jong PT. The risk and natural course of age-related maculopathy: follow-up at 6 1/2 years in the Rotterdam study. *Arch Ophthalmol.* 2003;121:519–526.
5. Bressler SB, Maguire MG, Bressler NM, Fine SL. Relationship of drusen and abnormalities of the retinal pigment epithelium to the

prognosis of neovascular macular degeneration. The Macular Photocoagulation Study Group. *Arch Ophthalmol.* 1990;108:1442–1447.

6. Klein R, Davis MD, Magli YL, Segal P, Klein BE, Hubbard L. The Wisconsin age-related maculopathy grading system. *Ophthalmology.* 1991;98:1128–1134.
7. The Age-Related Eye Disease Study system for classifying age-related macular degeneration from stereoscopic color fundus photographs: the Age-Related Eye Disease Study Report Number 6. *Am J Ophthalmol.* 2001;132:668–681.
8. Bird AC, Bressler NM, Bressler SB, et al. An international classification and grading system for age-related maculopathy and age-related macular degeneration. The International ARM Epidemiological Study Group. *Surv Ophthalmol.* 1995;39:367–374.
9. Smith RT, Chan JK, Nagasaki T, Sparrow JR, Barbazetto I. A method of drusen measurement based on reconstruction of fundus background reflectance. *Br J Ophthalmol.* 2005;89:87–91.
10. Shin DS, Javornik NB, Berger JW. Computer-assisted, interactive fundus image processing for macular drusen quantitation. *Ophthalmology.* 1999;106:1119–1125.
11. Drexler W, Sattmann H, Hermann B, et al. Enhanced visualization of macular pathology with the use of ultrahigh-resolution optical coherence tomography. *Arch Ophthalmol.* 2003;121:695–706.
12. Wojtkowski M, Srinivasan V, Fujimoto JG, et al. Three-dimensional retinal imaging with high-speed ultrahigh-resolution optical coherence tomography. *Ophthalmology.* 2005;112:1734–1746.
13. Srinivasan VJ, Wojtkowski M, Witkin AJ, et al. High-definition and 3-dimensional imaging of macular pathologies with high-speed ultrahigh-resolution optical coherence tomography. *Ophthalmology.* 2006;113:2054 e2051–e2014.
14. Pieroni CG, Witkin AJ, Ko TH, et al. Ultrahigh resolution optical coherence tomography in non-exudative age related macular degeneration. *Br J Ophthalmol.* 2006;90:191–197.
15. Khanifar AA, Koreishi AF, Izatt JA, Toth CA. Drusen ultrastructure imaging with spectral domain optical coherence tomography in age-related macular degeneration. *Ophthalmology.* 2008;115:1883–1890.
16. Schuman S, Koreishi A, Farsiu S, Jung S, Izatt J, Toth C. Photoreceptor layer thinning over drusen in eyes with age-related macular degeneration imaged in vivo with spectral-domain optical coherence tomography. *Ophthalmology.* 2009;116:488–496.
17. Jiao S, Knighton R, Huang X, Gregori G, Puliafito C. Simultaneous acquisition of sectional and fundus ophthalmic images with spectral-domain optical coherence tomography. *Opt Express.* 2005;13:444–452.
18. Stopa M, Bower BA, Davies E, Izatt JA, Toth CA. Correlation of pathologic features in spectral domain optical coherence tomography with conventional retinal studies. *Retina.* 2008;28:298–308.
19. Yi K, Mujat M, Park BH, et al. Spectral domain optical coherence tomography for quantitative evaluation of drusen and associated structural changes in non-neovascular age-related macular degeneration. *Br J Ophthalmol.* 2009;93:176–181.
20. Smith RT, Noah L, Jian C, Busuioc M, Laine AF. *Interactive Image Analysis in Age-Related Macular Degeneration* (*AMD*) *and Stargardt Disease* (*STGD*). Presented at the 42nd Asilomar Conference: Signals, Systems and Computers. Pacific Grove, CA: October 26–29, 2008. New York: IEEE Signal Processing Society; 2008;651–654.
21. Smith RT, Chan JK, Nagasaki T, et al. Automated detection of macular drusen using geometric background leveling and threshold selection. *Arch Ophthalmol.* 2005;123:200–206.
22. Hwang JC, Chan JW, Chang S, Smith RT. Predictive value of fundus autofluorescence for development of geographic atrophy in age-related macular degeneration. *Invest Ophthalmol Vis Sci.* 2006; 47:2655–2661.
23. Smith RT, Chan JK, Busuoic M, Sivagnanavel V, Bird AC, Chong NV. Autofluorescence characteristics of early, atrophic, and high-risk fellow eyes in age-related macular degeneration. *Invest Ophthalmol Vis Sci.* 2006;47:5495–5504.
24. Farsiu S, Chiu SJ, Izatt JA, Toth CA. *Fast Detection and Segmentation of Drusen in Retinal Optical Coherence Tomography Images.* San Jose, CA: Photonics West, Ophthalmic Technologies; 2008;68440D-68441-68412.
25. Xu C, Prince JL. Snakes, shapes, and gradient vector flow. *IEEE Trans Image Process.* 1998;7:359–369.
26. Takeda H, Farsiu S, Milanfar P. Kernel regression for image processing and reconstruction. *IEEE Trans Image Process.* 2007;16: 349–366.
27. Bland JM, Altman DG. Measuring agreement in method comparison studies. *Stat Methods Med Res.* 1999;8:135–160.
28. Klein ML, Ferris FL 3rd, Armstrong J, et al. Retinal precursors and the development of geographic atrophy in age-related macular degeneration. *Ophthalmology.* 2008;115:1026–1031.
29. Age-related eye disease study 2 ancillary spectral domain optical coherence tomography study. ClinicalTrials.gov Identifier: NCT00734487.